

Seven Cysteine-Deficient Mutants Depict the Interplay between Thermal and Chemical Stabilities of Individual Cysteine Residues in Mitogen-Activated Protein Kinase c-Jun N-Terminal Kinase 1

Tetsuko Nakaniwa,^{†,‡,||} Harumi Fukada,[§] Tatsuya Inoue,^{||} Masaki Gouda,[⊥] Ryoko Nakai,[⊥] Yasuyuki Kirii,[⊥] Motoyasu Adachi,[@] Taro Tamada,[@] Shin-ichi Segawa,[‡] Ryota Kuroki,[@] Toshiji Tada,^{||} and Takayoshi Kinoshita^{*,||}

[†]Department of Biological Sciences, Graduate School of Science, Osaka University, Toyonaka, Japan

[‡]Graduate School of Science and Technology, Kwansei Gakuin University, Sanda, Japan

[§]Graduate School of Life and Environmental Sciences, Osaka Prefecture University, Sakai, Japan

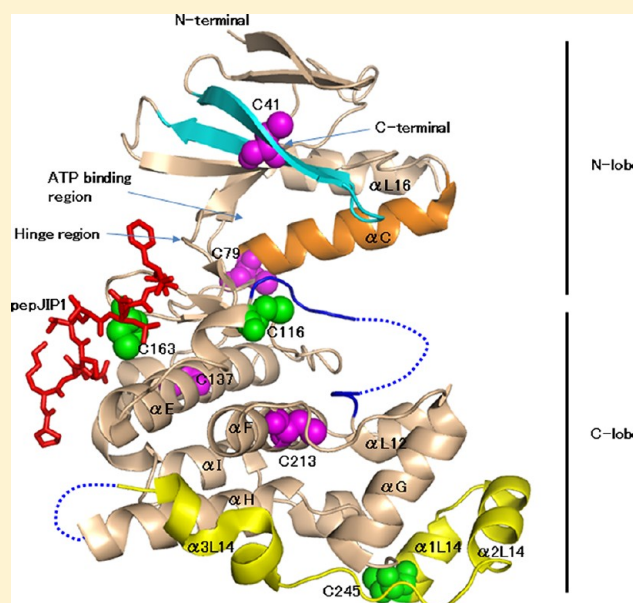
^{||}Graduate School of Science, Osaka Prefecture University, Sakai, Japan

[†]Carna Biosciences, Inc., Kobe, Japan

[@]Quantum Beam Science Directorate, Japan Atomic Energy Agency, Tokai, Japan

S Supporting Information

ABSTRACT: Intracellular proteins can have free cysteines that may contribute to their structure, function, and stability; however, free cysteines can lead to chemical instabilities in solution because of oxidation-driven aggregation. The MAP kinase, c-Jun N-terminal kinase 1 (JNK1), possesses seven free cysteines and is an important drug target for autoimmune diseases, cancers, and apoptosis-related diseases. To characterize the role of cysteine residues in the structure, function, and stability of JNK1, we prepared and evaluated wild-type JNK1 and seven cysteine-deficient JNK1 proteins. The nonreduced sodium dodecyl sulfate–polyacrylamide gel electrophoresis experiments showed that the chemical stability of JNK1 increased as the number of cysteines decreased. The contribution of each cysteine residue to biological function and thermal stability was highly susceptible to the environment surrounding the particular cysteine mutation. The mutations of solvent-exposed cysteine to serine did not influence biological function and increased the thermal stability. The mutation of the accessible cysteine involved in the hydrophobic pocket did not affect biological function, although a moderate thermal destabilization was observed. Cysteines in the loosely assembled hydrophobic environment moderately contributed to thermal stability, and the mutations of these cysteines had a negligible effect on enzyme activity. The other cysteines are involved in the tightly filled hydrophobic core, and mutation of these residues was found to correlate with thermal stability and enzyme activity. These findings about the role of cysteine residues should allow us to obtain a stable JNK1 and thus promote the discovery of potent JNK1 inhibitors.



Free cysteine residues in cytosolic proteins usually contribute to their biological function, structure, and stability. A cysteine residue in several enzymes, including cysteine proteases, thioredoxin, and peroxiredoxin, acts as an active center,^{1,2} whereas a cysteine present in several regulatory proteins acts as a molecular switch via chemical modification such as S-nitrosylation and S-glutathionylation.^{3,4} As such, the sulfhydryl group of a cysteine residue displays nucleophilic reactivity essential for physiological reactions but can also give rise to chemical instability. Conversely, several protein structures have shown that the hydrophobic character of cysteine

residues stabilizes the conformation of the protein by forming part of the hydrophobic core. Cytosolic protein c-Jun N-terminal kinase 1 (JNK1) possesses seven free cysteine residues that perhaps affect its function, structure, and stability.

The c-Jun N-terminal kinases (JNKs) are members of the mitogen-activated protein kinase (MAPK) family, and they can

Received: July 10, 2012

Revised: September 28, 2012

Published: September 29, 2012

be activated by the upstream kinases MKK4 and MKK7 in response to various stimuli such as environmental stress, cytokines, and fatty acids.^{5,6} There is a growing body of evidence indicating that the adverse activation of JNK1 is found in a wide variety of human diseases such as diabetes, cardiovascular diseases, autoimmune diseases, and tumorigenesis.^{7–12} Over the past decade, there has been considerable effort made to identify JNK inhibitors suitable for clinical development.^{13–16} Several inhibitors were developed through structure-based drug design (SBDD) by referring to the crystal structures of the JNK1-potent inhibitor complexes.^{15–17}

JNK1 is a cytosolic protein that contains free cysteine residues that are primarily used as hydrophobic amino acids to maintain its tertiary structure. However, JNK1 is significantly impaired by oxidation-driven aggregation in an aerobic environment. Free sulfhydryl groups in proteins occasionally form non-native intra- and/or intermolecular disulfide bonds that lead to denatured aggregation and thus give rise to adverse effects during physicochemical experiments. An approach to improving the molecular characteristics of a kinase is to exchange the free cysteine residues with a different amino acid. There are several examples for replacement of a cysteine residue with a different amino acid for the prevention of aggregation. Rational surface modification^{18,19} and substitution of nonessential free cysteine residues^{20–24} allow the production of samples with higher chemical stability, specific activity, and homogeneity and thus overcome crystallization problems. In a MAP kinase p38 α study, a single-point mutation of a cysteine residue (C162S) located on the protein surface, which is conserved in JNK1, also moderated aggregation and improved the homogeneity and chemical stability of the enzyme.²⁵ However, the p38 α C162S mutant had significantly attenuated enzyme activity when compared with that of the wild-type protein. The C117S/C222S double mutation of JNK2 also reduced the level of aggregation compared with that of the wild-type species.²⁶ These observations indicate that some cysteine residues on the molecular surface of MAP kinases confer chemical instability but make a negligible contribution to biological function and structure. Two issues describing the roles of cysteine residues in MAP kinases remain unresolved. (i) Do all surface cysteine residues behave like the aforementioned surface cysteine residues? (ii) How do the buried cysteine residues contribute to their function, stability, and structure? Thus, the global analyses of the free cysteine residues of a kinase with respect to chemical stabilization, biological activity, and thermal stability would provide significant insight into the role of cysteine residues in MAP kinases as well as other cytosolic proteins. Moreover, the replacement of cysteine residues with other amino acid residues that stabilize this kinase mutant will contribute to the production of proteins that are useful for drug screening by physicochemical experiments. The ability to complete physicochemical experiments such as thermodynamic analysis and binding assays using nuclear magnetic resonance and surface plasmon resonance would greatly potentiate the SBDD strategy.

Wild-type JNK1 contains seven free cysteine residues that were divided into accessible surface residues (Cys116, Cys163, and Cys245) and fully buried residues (Cys41, Cys79, Cys137, and Cys213) (Table 1). However, it is unknown how each cysteine substitution impacts the chemical and thermal stabilities and enzyme activity of JNK1. Therefore, to obtain a comprehensive understanding of the individual cysteine-deficient effects, we prepared the wild-type protein and seven cysteine-deficient mutants and evaluated each construct by biological, chemical, thermal, and structural analyses.

Table 1. Accessible Surface Areas (ASAs) of Cysteine Residues^a

residue	total ASA (Å ²)	main chain ASA (Å ²)	side chain ASA (Å ²)	sulfate atom ASA (Å ²)
Cys41	0	0	0	0
Cys79	32.9	21.8	11.1	0
Cys116	49.5	2.9	46.6	26.6
Cys137	0.4	0.4	0	0
Cys163	20.2	4.9	15.3	2.9
Cys213	0	0	0	0
Cys245	67.9	4.5	63.4	57.7

^aAll accessible surface areas (ASAs) of each cysteine residue were calculated using a high-resolution JNK1 structure (Protein Data Bank entry 3elj) by the *Surface Racer* program.⁴⁰

MATERIALS AND METHODS

Protein Preparation. The codon-optimized human JNK1 β 1 isoform (residues 1–364) gene (M0) was fully synthesized (TAKARA BIO Inc., Otsu, Japan) and cloned into the pET24a expression vector (Merck Millipore, Billerica, MA) at the NdeI and XhoI sites, resulting in a construct with a His₆ purification-tagged at the C-terminus. Seven cysteine-deficient JNK1 mutants (M1–M7) were prepared by the QuickChange system (Stratagene, Santa Clara, CA), using a previously described method.²⁵ *Escherichia coli* BL21(DE3) cells (Merck Millipore) were transformed by the cloned vector, including M0 or the respective mutants, and grown at 37 °C using LB medium containing 100 μ g/mL ampicillin until the OD₆₀₀ reached 0.5. The temperature of the cultivated broth was then decreased to 25 °C, and protein was induced by the addition of IPTG to a final concentration of 0.3 mM. After overnight expression at 25 °C, cells were harvested by centrifugation, resuspended in a lysis buffer consisting of 20 mM Tris (pH 7.5), 500 mM NaCl, and 20 mM imidazole, and frozen at –80 °C. The cell pellet was sonicated for 15 min on ice, and the cell debris was removed by centrifugation at 10000g for 30 min at 4 °C. The supernatant was loaded onto a 1 mL bed volume of a Ni-NTA Superflow-Cartridge column (Quiagen, Hilden, Germany) that had previously been equilibrated in lysis buffer. After being washed with lysis buffer, the protein was eluted with a buffer containing 20 mM Tris (pH 7.5), 500 mM NaCl, and 250 mM imidazole. DTT (2 mM) was immediately added to the pooled fractions. The fraction was further purified by gel filtration using a HiPrep 16/60 Sephacryl S-200 HR column (GE Healthcare, Little Chalfont, U.K.) that was equilibrated with 20 mM Tris (pH 7.5), 250 mM NaCl, 5% (v/v) glycerol, and 5 mM DTT. Eluted peak fractions were pooled, and the protein was concentrated to 10 mg/mL using a Centrprep YM-10 filter unit (Merck Millipore). The total protein concentration was determined by the Bradford method.²⁷ However, the protein preparation for the nonreduced sodium dodecyl sulfate–polyacrylamide gel electrophoresis (SDS–PAGE) and differential scanning calorimetry experiments was performed without the reducing agent.

Enzyme Activity Measurement. Purified JNK1 was activated by incubation of a mixture composed of 20 μ M JNK1, 0.4 μ M active MAP2K4 (HumanZyme, Inc., Chicago, IL), 0.4 μ M active MAP2K7 (HumanZyme, Inc.), 1 mM ATP, and 5 mM MgCl₂ in assay buffer A [20 mM HEPES (pH 7.5), 0.01% Tween 20, and 2 mM DTT] at 25 °C for 1 h. The activated JNK1 solution was diluted to 100 nM with assay buffer A and mixed with the substrate solution containing 10 mM MgCl₂, 2 mM ATP, and 2 μ M FITC-labeled peptide substrate

(Carna Biosciences, Inc.). The reaction was conducted at 25 °C for 1 h. The JNK1 kinase activity was determined by the off-chip mobility shift assay (MSA) using the LabChip3000 (Caliper Life Sciences, Hopkinton, MA). Kinase reactions were terminated by EDTA and the read-out by an EX Reader II. The amounts (peak height) of phosphorylated (*P*) and nonphosphorylated (*S*) peptide substrates were measured, and the phosphorylation rate of the substrate was defined by $P/(P + S)$ as the enzyme activity.

Nonreduced SDS–PAGE Experiments. The chemical stabilities of the purified JNK1 protein samples were evaluated by nonreduced SDS–PAGE using 12.5% polyacrylamide gels. Gels were stained with Bio Safe Coomassie (Bio-Rad, Hercules, CA). For the evaluation of the time and temperature dependencies against oxidation, the protein samples were concentrated to 0.4 mg/mL and incubated at 4 and 20 °C in the reducing agent-free buffer containing 250 mM NaCl, 5% glycerol, and 20 mM Tris-HCl (pH 7.5) for 0, 12, 24, and 36 h before the SDS–PAGE experiments.

Differential Scanning Calorimetry (DSC). The thermal unfolding of JNK1 was measured by a differential scanning calorimeter, Nano DSC (TA Instruments Inc., New Castle, DE), with platinum tubing cells having a volume of 0.3 mL. The wild-type protein or each mutant was concentrated to 23 μ M in the experimental buffer containing 250 mM NaCl and 20 mM phosphate (pH 7.5). Temperature scans were performed from 10 to 100 °C at a scan rate of 60 °C/h. For evaluating the thermal stability enhancements by the peptide fragment from JIP1 on M0, M3, and M7, the protein concentration was adjusted to 23 μ M. The protein was then mixed directly with the peptide with the RPKRPTTLNLF sequence (Scrum Inc., Tokyo, Japan) at a molar ratio of 1:5 and incubated on ice for 4 h to allow formation of the complex. Temperature scans of these complexes were performed using the same procedure used to characterize the apoprotein. DSC curves were analyzed on the basis of the van't Hoff equation using the curve resolution technique.²⁸

Structure Analysis. The seven cysteine-deficient mutants (M1–M7) were individually concentrated for crystallization to 5 mg/mL. The concentration was confirmed by the Bradford method.²⁷ Before the crystallization trial, the purified protein was mixed with the peptide fragment from JIP1 at a molar ratio of 1:5 and incubated on ice for 4 h to allow formation of the complex. Crystals of the mutants were obtained by the sitting drop vapor diffusion method at 4 °C with a reservoir of 2.2 M ammonium sulfate, 0.2 M sodium chloride, and 0.1 M sodium cacodylate (pH 6.5). The crystallization drop contained 2 μ L of the protein solution and 2 μ L of the reservoir solution. The crystals were dipped into the reservoir solution that included 15% glycerol as a cryoprotectant, and a nitrogen gas stream at 100 K was used to freeze the crystals. Diffraction data for the M2–M7 mutants were collected on a CCD Quantum 270 detector (ADSC, San Diego, CA) at a wavelength of 1.00 Å using the synchrotron radiation at Accumulator Ring beamline NE3A of the Photon Factory. The M1 mutant diffraction data were collected on a Raxis-IV⁺⁺ imaging plate system (Rigaku, Tokyo, Japan) using monochromatized Cu K α radiation generated with a MicroMax-HF007 instrument (Rigaku). All data sets were processed and scaled using HKL2000.²⁹ The structures were determined by molecular replacement using MOLREP³⁰ and refined with REFMAC³¹ in the CCP4 program suite. Manual model corrections were performed with COOT.³² The structures of the mutants were validated with PROCHECK.³³ Figures were generated with PyMOL (DeLano Scientific, San Francisco, CA), and structural comparison was conducted using LSQKAB.³¹ Data collection

and refinement statistics are summarized in Table S1 of the Supporting Information. Coordinates for the seven cysteine-deficient mutant structures have been deposited in the PDB as entries 3VUD, 3VUG, 3VUH, 3VUI, 3VUK, 3VUL, and 3VUM.

RESULTS

Construct Design of the Seven Cysteine-Deficient Mutants. JNK1 possesses seven cysteine residues divided into two groups: accessible residues, including Cys116, Cys163, and Cys245, and (ii) fully buried residues, including Cys41, Cys79, Cys137, and Cys213 (Figure 1 and Table 1) based upon the 1.8 Å

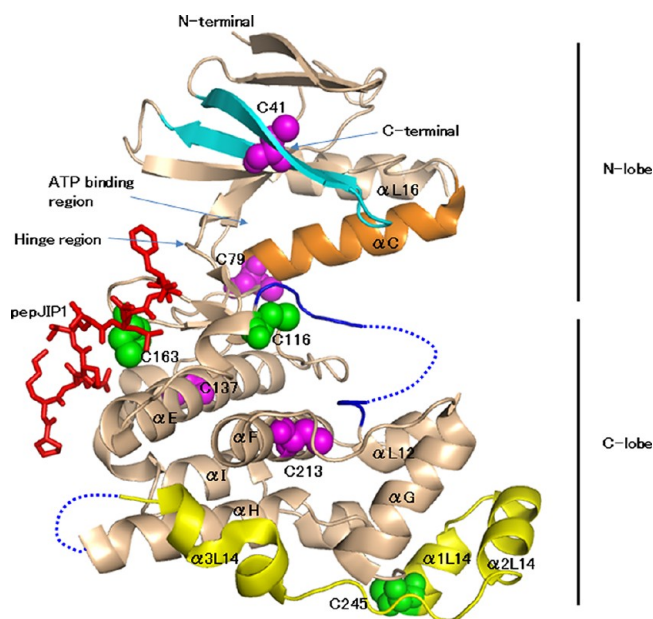


Figure 1. JNK1 structure and cysteine residue sites (PDB entry 1UKH). Surface cysteine residues (C116, C163, and C245) are depicted as green spheres and buried cysteine residues (C41, C79, C137, and C213) as magenta spheres. The pepJIP1 peptide is depicted as a red stick model. The glycine-rich loop is colored cyan, the MAP kinase insert yellow, helix α C orange, and the activation loop blue. The disordered regions are represented by the blue dashed lines.

wild-type structure.¹⁷ We postulate that the cysteines are the most adverse factor for the oxidation-driven aggregation of wild-type JNK1 (M0). In a p38 α MAP kinase study, a surface cysteine-deficient mutation moderated the aggregation and improved the homogeneity and stability of the enzyme.²⁵ Therefore, we prepared seven cysteine-deficient mutants in an effort to improve the chemical stability of JNK1 [M1–M7 (Table 2)]. M1 was mutated at Cys245, whereas M2 was mutated at Cys116 in addition to the M1 mutation. Further mutations involved sequentially introducing mutations to other cysteine residues. Thus, the M7 mutant had no cysteine residues. The surface cysteine residues Cys116 and Cys245 had primary and secondary accessibilities, respectively (Table 1), and were mutated to serine because this mutation was expected to improve solubility. The other surface cysteine residue, Cys163, forms a hydrophobic pocket to allosterically recognize the substrate peptide.³⁴ Cys163 of JNK1 was therefore mutated to alanine because the C163S mutation would likely attenuate enzyme activity, as observed for p38 α .²⁵ The C162S mutation in p38 α was considered to disrupt the hydrophobic pocket and adversely affect the binding of the substrate peptide. Furthermore, the C163V mutation of JNK1

Table 2. Sequence Positions of the Substituted Cysteine Residues

	C245S	C116S	C163A	C79V	C137V	C213V	C41V
M1	+						
M2	+	+					
M3	+	+	+				
M4	+	+	+	+			
M5	+	+	+	+	+		
M6	+	+	+	+	+	+	
M7	+	+	+	+	+	+	+

seemed to sterically interfere with substrate recognition based upon the pepJIP1 complex structure.¹⁷ The four fully buried cysteine residues, Cys79, Cys137, Cys213, and Cys41, were mutated to valine because these residues exist in the hydrophobic core and valine is similar in size to cysteine.^{23,35–37} This paper inspected the effect of the cysteine-deficient mutations on the chemical and thermal stability of the protein by comparing wild type M0 and mutants M1–M7.

Protein Production Yield for the Wild Type and Seven Cysteine-Deficient Mutants. To compare the wild type (M0) with the seven mutants (M1–M7) in expression, all genes were identically cloned into the pET24a vector and the proteins were expressed under exactly the same conditions. The SDS–PAGE experiments revealed that all mutants were expressed at levels similar to those of M0 (Figure 2a). The soluble fractions of M1–M5 contained significantly more of the target protein than the respective insoluble fractions, whereas both fractions of M0 had equal amounts of protein (Figure 2b,c). M3 and M4 were mainly present in the soluble fraction. M6 and M7 were primarily expressed as insoluble material (Figure 2b,c).

M0 and cysteine-deficient mutants M1–M7 were purified using the same procedure. The use of Ni-NTA chromatography gave approximately 60–70% pure target proteins, as judged using a densitometer from the 50 mL of cultivated broth. Size exclusion chromatography of the Ni-purified M0 and cysteine-deficient mutants revealed a single peak corresponding to the monomeric enzyme. All cysteine-deficient mutants conferred a higher-production yield than 1.0 mg of the wild-type protein: 1.6 mg of M1, 1.7 mg of M2, 3.8 mg of M3, 3.0 mg of M4, 2.4 mg of M5, 1.4 mg of M6, and 1.2 mg of M7 (Table S2 of the Supporting Information). The final production yield of M3 and M4 was not less than 3-fold higher compared with that of M0.

Oxidation-Driven Oligomerization of the Wild Type and Cysteine-Deficient Mutants. The chemical stability of the JNK1 proteins was evaluated by nonreducing SDS–PAGE by measurement every 12 h for 36 h at 4 and 20 °C. The laddering bands revealed that M0–M2 formed dimers, trimers, and probably tetramers by intermolecular disulfide bonding (Figure 3).

M0 with seven cysteine residues indicated the largest oligomeric distribution that increased in a time- and temperature-dependent manner (Figure 3a). A similar phenomenon for other enzymes possessing cysteine residues has been reported previously.^{21,22,34} M0 immediately started to dimerize and after incubation for 12 h at 4 °C also formed trimers (Figure 3a). Compared with M0, M1 and M2 showed a gradual reduction in the oligomeric distribution and predominantly formed the trimer rather than the dimer (Figure 3a–c). In addition, the amounts of the M2 tetramer and oligomer drastically increased during the 24–36 h period at 4 °C (Figure 3c). Conversely, M3–M5 hardly oligomerized, and their oligomer distribution did not increase in a time- or temperature-dependent manner, although trace amounts of trimers were detected in those mutants (Figure 3d–f). A small amount of the M3 trimer was observed after 36 h at 4 °C (Figure 3d). The M6 dimer was detected, but the amount did not increase in a time- and temperature-dependent manner (Figure 3g). As expected, M7 possessing no cysteine residues was the most stable against disulfide oxidation and remained monomeric (Figure 3h).

Together, the all cysteine-deficient mutants (M1–M7) were more chemically stable than the wild-type protein (M0). In particular, M3–M5 and M7 were found to be sufficiently stable to perform the time-consuming physicochemical experiments.

Enzyme Activity of the Wild Type and Cysteine-Deficient Mutants. Recombinant JNK1 was in the inactive state and was activated by upstream kinases, MKK4 and MKK7, before the enzyme assay. The specific activity of JNK1 presented in Table 3 was defined by the amount of phosphate transferred to the FITC-labeled substrate peptide per minute per milligram of protein.

The kinase activities of M0 and the cysteine-deficient mutants were determined by their ability to phosphorylate the substrate peptide using the microfluidics-based mobility shift assay approach. M0 and all mutants showed time- and dose-dependent increases in the rates of phosphorylation of the substrate. Four mutants (M1–M4) exhibited kinase activity comparable to that of M0 with relative activities of 110, 98, 96, and 95%, respectively (Table 3). In contrast, M5 displayed a kinase activity of 67% relative to the activity of M0. The kinase activities were found to be even further attenuated for M6 and M7, with relative values of 23 and 24%, respectively, compared with the activity of the wild-type protein (Table 3).

Thermal Stability of the Wild Type and Cysteine-Deficient Mutants. The thermal stability of the wild type and each mutant was evaluated by DSC measurements in the apo state with the same procedure. All proteins irreversibly unfolded via a similar process that has a three-state transition model via an intermediate state (Figure 4). The deconvolution analyses of each DSC curve conferred the thermal denaturation midpoint (T_m) and van't Hoff enthalpy change (ΔH) (Table 3). T_{m1} and

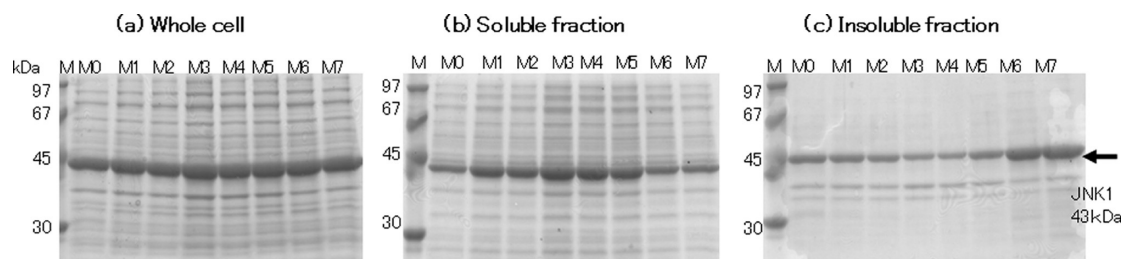


Figure 2. SDS–PAGE showing the productivity of JNK1 proteins by bacteria. Columns marked with an M contained molecular weight markers. (a) Whole cell proteins after induction. (b) Soluble fraction after induction. (c) Insoluble fraction after induction.

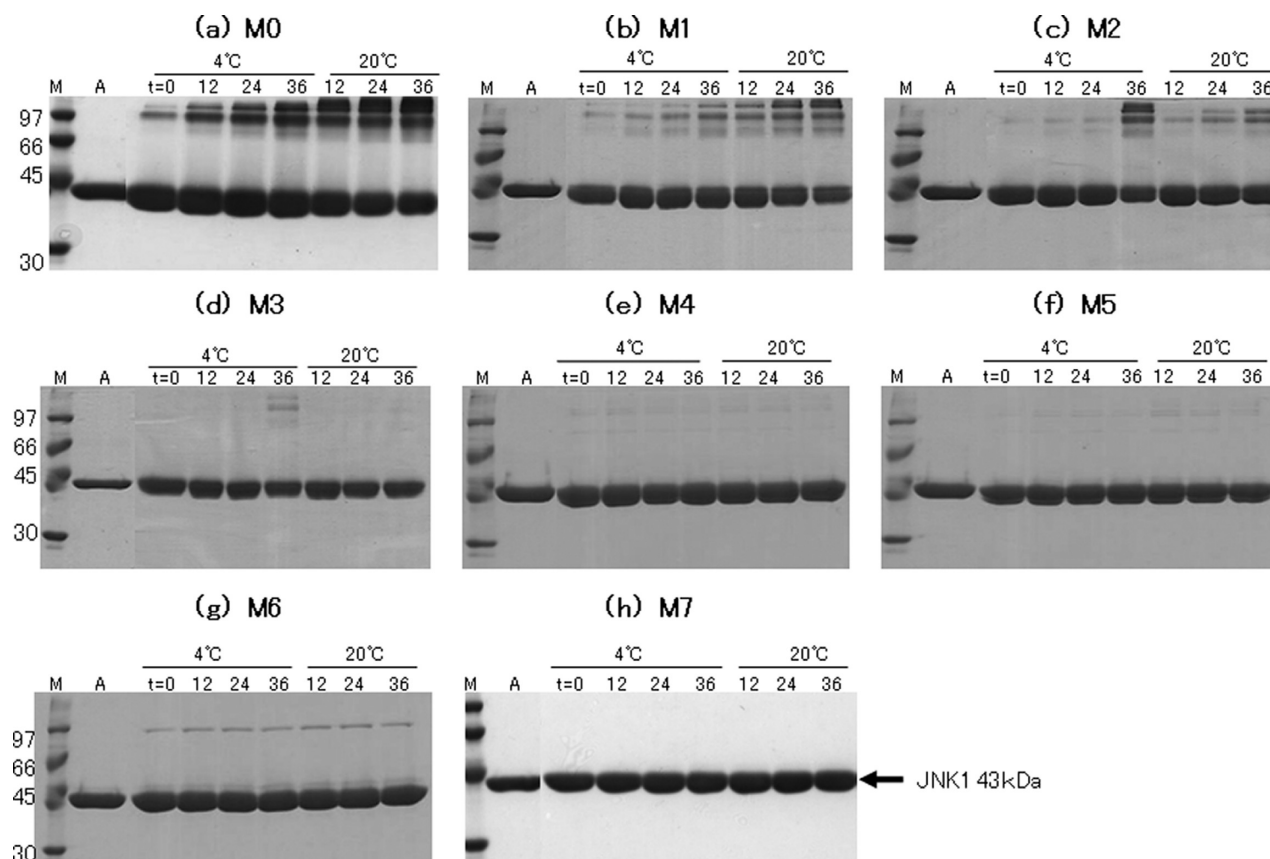


Figure 3. Nonreduced SDS–PAGE of the wild type (M0) and the cysteine-deficient mutants (M1–M7) incubated under nonreducing conditions. M0 and seven cysteine-deficient mutants were incubated in 250 mM NaCl, 5% glycerol, and 20 mM Tris-HCl (pH 7.5). The sample concentration was 0.4 mg/mL; the incubation temperatures were 4 and 20 °C, and the incubation times were 0, 12, 24, and 36 h.

Table 3. Enzymatic Activities and Thermal Stabilities of Wild-Type JNK1 and the Seven Cysteine Mutants^a

	M0	M1 (C245S)	M2 (C116S)	M3 (C163A)	M4 (C79V)	M5 (C137V)	M6 (C213V)	M7 (C41V)
relative activity (%) ^b	100	110 (+10)	99 (−11)	96 (−3)	95 (−1)	67 (−28)	23 (−44)	24 (+1)
T_{m1} (°C) ^c	46.2	47.8 (+1.6)	49.5 (+1.7)	47.8 (−1.7)	47.2 (−0.6)	44.5 (−2.7)	42.8 (−1.7)	41.3 (−1.5)
T_{m2} (°C) ^c	54.1	53.6 (−0.5)	53.9 (+0.3)	53.5 (−0.4)	50 (−3.5)	50.4 (+0.4)	50.4 (0.0)	50 (−0.4)
ΔH_1 (kJ/mol) ^d	477	651 (+174)	793 (+142)	672 (−121)	765 (+93)	682 (−83)	436 (−246)	367 (−69)
ΔH_2 (kJ/mol) ^d	380	435 (+55)	535 (+100)	388 (−147)	449 (+61)	385 (−64)	356 (−29)	272 (−84)

^a T_m and ΔH values of M0 and all mutants from fits of a two-state transition model to the DSC data. Values in parentheses are for the delta values due to the additional mutation. ^bThe JNK1 activity was measured at 25 °C for 1 h by incubating a mixture composed of 20 μ M JNK1, two upstream kinases (0.4 μ M active MAP2K4 and 0.4 μ M active MAP2K7), 1 mM ATP, and 5 mM MgCl₂ in assay buffer [20 mM HEPES (pH 7.5), 0.01% Tween 20, and 2 mM DTT]. The activated JNK1 solution was diluted with assay buffer and mixed with the 2-fold substrate solution (10 mM MgCl₂, 2 mM ATP, and 2 μ M FITC-labeled peptide substrate) at 25 °C for 1 h. The amount of unphosphorylated and phosphorylated substrate peptides was repeatedly detected by the microfluidics-based mobility shift assay (Caliper LC3000 System, Caliper Life Sciences). The specific activity of JNK1 was defined by the amount (moles) of phosphate transferred to the FITC-labeled substrate peptides per minute per milligram of protein. The relative activity is indicated as the value relative to the specific activity of M0. ^cThermal denaturation midpoint. ^dvan't Hoff enthalpy change.

ΔH_1 were assigned as parameters for the lower-temperature transition (T_{m1} transition) and T_{m2} and ΔH_2 for the higher-temperature transition (T_{m2} transition). The T_{m1} values for M1 (47.8 °C), M2 (49.5 °C), M3 (47.8 °C), and M4 (47.2 °C) were significantly higher than the T_{m1} value of 46.2 °C for M0 (Table 3). M2 gave the highest T_{m1} value, and M1 and M3 were ranked as second-order with respect to the T_{m1} value. The values of 44.5 °C (M5), 42.8 °C (M6), and 41.3 °C (M7) were considerably lower than the wild-type T_{m1} value. All T_{m1} values roughly represented a positive correlation with the ΔH_1 values (Table 3). The T_{m2} values were divided into two distinct groups and had no correlation with the ΔH_2 values (Table 3). The T_{m2} values of 53.6 °C (M1),

53.9 °C (M2), and 53.5 °C (M3) were similar to that of 54.1 °C for M0; however, those of 50.0 °C (M4), 50.4 °C (M5), 50.4 °C (M6), and 50.0 °C (M7) were markedly lower than the value for the wild-type protein.

Peptide-Driven Thermal Stability Enhancement of M0, M3, and M7. The thermal stability enhancement of M0, M3, and M7 upon binding the peptide fragment of scaffold protein JIP1 (pepJIP1), which binds to specifically the C-lobe domain,³⁴ was observed by DSC experiments. The peptide elevated the transition temperature T_{m1} by 4.5 °C for M0, 1.9 °C for M3, and 2.3 °C for M7; however, no change in the T_{m2} values was observed (Table S3 of the Supporting Information). The T_{m1} value of M0 was

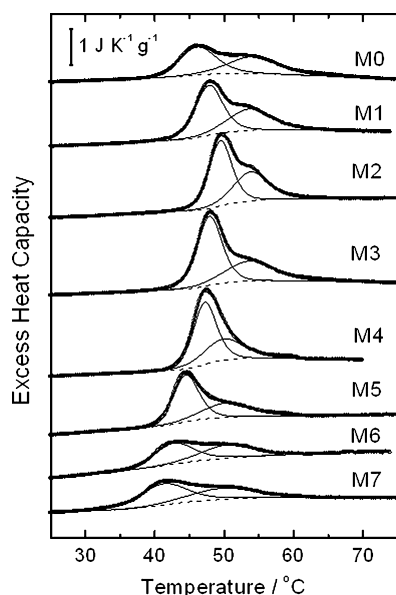


Figure 4. DSC curves for the wild-type protein and the cysteine mutants. The thick lines represent the raw DSC curves and the thin lines the deconvoluted DSC curves.

elevated more strongly than that of M3. Furthermore, the peptide considerably sharpened the exothermic peak in transition temperature T_{m1} but had little effect on the peak shape in the T_{m2} transition temperatures of M0, M3, and M7 (Figure 5).

Crystal Structures of the Seven Cysteine-Deficient Mutants. To evaluate the effect of the cysteine-deficient mutations on protein thermal stability, the crystal structures of the seven mutants in complex with the pepJIP1 peptide, which was essential to crystallization of JNK1, were determined to resolutions between 2.69 and 3.5 Å (Table S1 of the Supporting Information). The structures were compared with each other and the wild-type high-resolution structure previously reported.¹⁷ All mutant structures were generally well-defined, including the mutation sites; however, some undefined regions did exist. In all structures, the six residues at the N-terminus and the three residues at the C-terminus were disordered. Additionally, three residues (180–182) within the activation loop in the structures of M1–M5 were disordered, and the activation loop region of those structures was highly ordered and participated in crystal packing. In the structures of M6 and M7, 13 residues (175–187) in the active loop were disordered in addition to the two terminal regions discussed above.

The conformation of the M1–M7 mutants adopted a two-lobe folding motif that is canonical for protein kinases (Figure 1) as well as wild-type JNK1 (PDB entry 1UKH). The N-terminal lobe of each mutant largely consisted of β -strands, and the C-terminal lobe was primarily α -helical. Both lobes were connected by the so-called hinge region (residues 109–113), which is vital to ATP binding. In addition, all mutants conserved the insertion and extension structures that are characteristic of the MAP kinase family: an N-terminal β -hairpin, an extended loop region containing two α -helices, termed the MAP kinase insertion domain, and a C-terminal α -helix. Superimposition of the seven cysteine-deficient mutants on the wild-type structure showed that there were conformational differences in two regions (Figure 6a). In one region, a structured α -helix in the wild type was a loop structure in the mutants (Figure 6a). In this region, the carboxyl group of Glu285 in the looped region forms a salt bridge to the

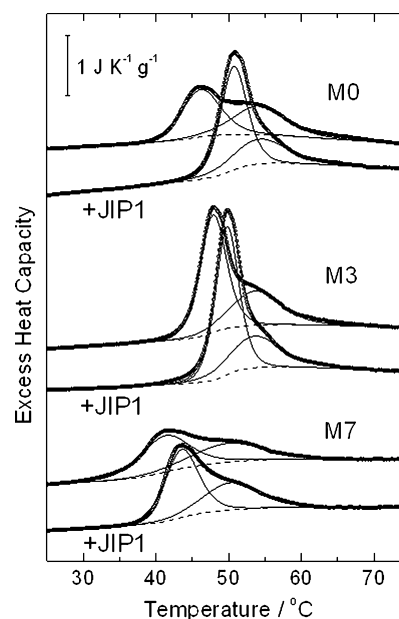


Figure 5. Deconvoluted DSC curves for M0, M3, and M7 with and without the pepJIP1 peptide. The thick lines represent the raw DSC curves and the thin lines the deconvoluted DSC curves.

amine group of Lys24 in the crystal-symmetric molecule (Figure 6b). This interaction was conserved in the mutants, although they possessed distinct crystal packing effects (Table S1 of the Supporting Information). In the other region known as the MAP kinase insertion, the loop structure of M6 and M7 opened toward the solvent region, whereas for the structures of M1–M5, the conformation of this region was similar to that of the wild-type protein (Figure 6a,c). The C213V mutation site proximate to the MAP kinase insertion caused a large conformational change by altering the hydrogen bond network because of the side chain flipping of Arg189 and Tyr190 in the activation loop (Figure 6c).

A brief description of structural changes at the seven mutation sites follows (Figure 7). The first surface mutation (C245S) was manipulated in the α 1L14-helix of the MAP kinase insertion region of the C-lobe domain (Figure 1). In the wild-type structure (PDB entry 3elj), Cys245 was exposed to the solvent and possessed a double conformation of the thiol group, which formed no significant intramolecular interactions (Figure 7a). On the other hand, the hydroxyl group of Ser245 in the M1 mutant, as well as the other mutants, was located in the narrow space in which the larger S γ atom of Cys245 could not be located. Furthermore, the hydroxyl group made two new hydrogen bonds with the backbone NH group of Glu247 and Phe248 at the terminus of α 1L14 (Figure 7a).

The second surface mutation (C116S) was in the flexible region proximate to the hinge region. In the structures of M1 and M0, Cys116 was largely accessible to the solvent and formed no significant intramolecular interactions with other residues (Figure 7b). On the other hand, the hydroxyl group of Ser116 of M2–M7 rotated to and made a hydrogen bond with the side chain of Gln117 (Figure 7b).

Cys163 is located on the protein surface but serves as a corner of the hydrophobic pocket that plays an important role in recognizing a hydrophobic amino acid of the scaffold protein, such as JIP1 and the substrate protein. The C163A mutation created the void volume in the hydrophobic substrate-recognizing

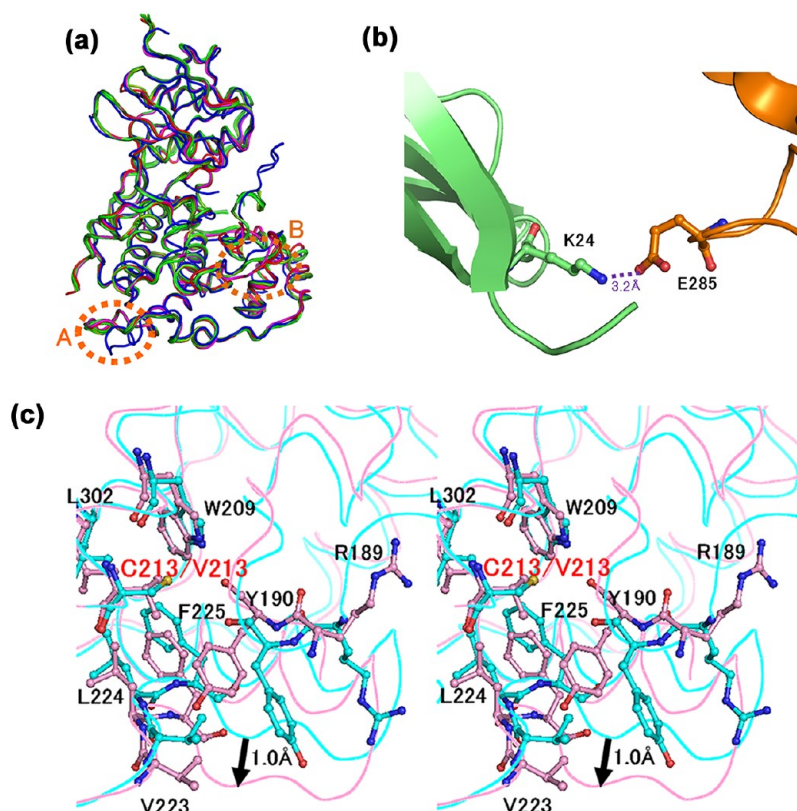


Figure 6. Comparison of the wild-type JNK1 structure with the seven cysteine-deficient mutant structures. (a) Superimposition of the seven cysteine-deficient mutant structures on the wild-type (blue) structure. Two regions, A and B, of the mutants, possessing a distinct conformation when compared with that of the wild type, are denoted with orange circles. (b) Salt bridge due to crystal packing in region A. Two crystal-symmetric molecules in the M3 crystal are colored orange and green. The hydrogen bond is represented by a dashed line. (c) Stereoview of region B proximate to C213V. M3 is colored cyan and M7 pink. The arrow shows that the loop structure of M7 has moved away by ~ 1 Å when compared with the structure of M3.

pocket involving Leu115, Val118, Met121, Leu123, Arg127, Leu131, and Val159 (Figure 7c).

Cys79 is located at the end of helix α C and forms a double conformation with respect to the thiol group that interacts with Ile337 or Pro338 in the C-terminal extension segment in the wild-type JNK1 structure (PDB entry 3elj) (Figure 7d). However, in the structures of M4–M7, the $C\gamma$ atom of Val79 possibly creates repulsive forces with the backbone carbonyl O atom of Lys336 in the C-terminal extension and thereby pushed away this region (Figure 7d).

The thiol group of Cys137 located on helix α E formed the snugly packed hydrophobic cluster cooperating with the side chains of Tyr133, Leu316, and Ala330 in the wild-type and M1–M4 structures (Figure 7e). The thiol group of Cys137 also formed an SH– π interaction with Tyr133 (Figure 7e). In the vicinity of Cys137, a salt bridge between Lys83 and Glu329 and a hydrogen bond network involving Tyr133, Trp324, Asp326, and Glu329 were formed and perhaps contributed to the maintenance of the C-terminal lobe configuration (Figure 7e). The $O\eta$ atom of Tyr133 made four hydrogen bonds with the backbone carbonyl O atom of Trp324, the backbone NH group and the backbone carbonyl O atom of Asp326, and the $O\epsilon$ atom of Glu329 that formed a salt bridge with the $N\psi$ atom of Lys83 on the top of the long loop in the vicinity of helix α C (Figure 7e). The structures of M5–M7 showed that the C137V mutation destroyed the hydrophobic cluster and sequentially the salt bridge.

Cys213 is located on helix α F near the activation loop and forms part of a tightly filled hydrophobic cluster cooperating with Trp209, Val223, Leu224, Phe225, and Leu302 in the wild-type

and M1–M5 structures (Figure 6c). Furthermore, its proximate region forms a hydrogen bond network consisting of three hydrogen bonds involving the activation loop that regulates enzyme activity (Figure 7f). The $O\eta$ atom of Tyr191 in the activation loop made a hydrogen bond with the $O\epsilon$ atom of Glu217 in helix α F (Figure 7f). The $N\eta$ atom and backbone NH group of Arg189 in the activation loop make two hydrogen bonds with the backbone carbonyl O atom of Thr228 in the α F– α G loop and with the backbone carbonyl O atom of Gly227, respectively (Figure 7f). In the structures of M6 and M7, the hydrophobic core was pushed away by ~ 1.0 Å when compared with the wild-type and M1–M5 structures, and thereby, the hydrogen network was broken (Figure 6c).

Cys41 is located on strand β 4 in the glycine-rich loop, a flexible region that functions as the on–off switch of ATP binding, and Cys41 is loosely surrounded by the hydrophobic amino acids Ile15, Phe20, Leu29, Pro31, and Ala42 in M6 (Figure 7g). Val41 in the M7 mutant was accommodated by these hydrophobic residues.

DISCUSSION

Effect of Each Cysteine Mutation on the Stability and Function of JNK1. The first surface mutation (C245S in M1) markedly augmented the T_{m1} value but not T_{m2} , as well as retaining kinase activity (Table 3). The T_{m1} transition was stabilized by this mutation in an enthalpy-driven manner (Table 3). The thermal stabilization was likely acquired by the appended hydrogen bonds of S245 (Figure 7a). However, the C245S single mutation was insufficient to stabilize the chemical properties of JNK1 and to enhance production yields but resulted in slight increase in enzyme activity.

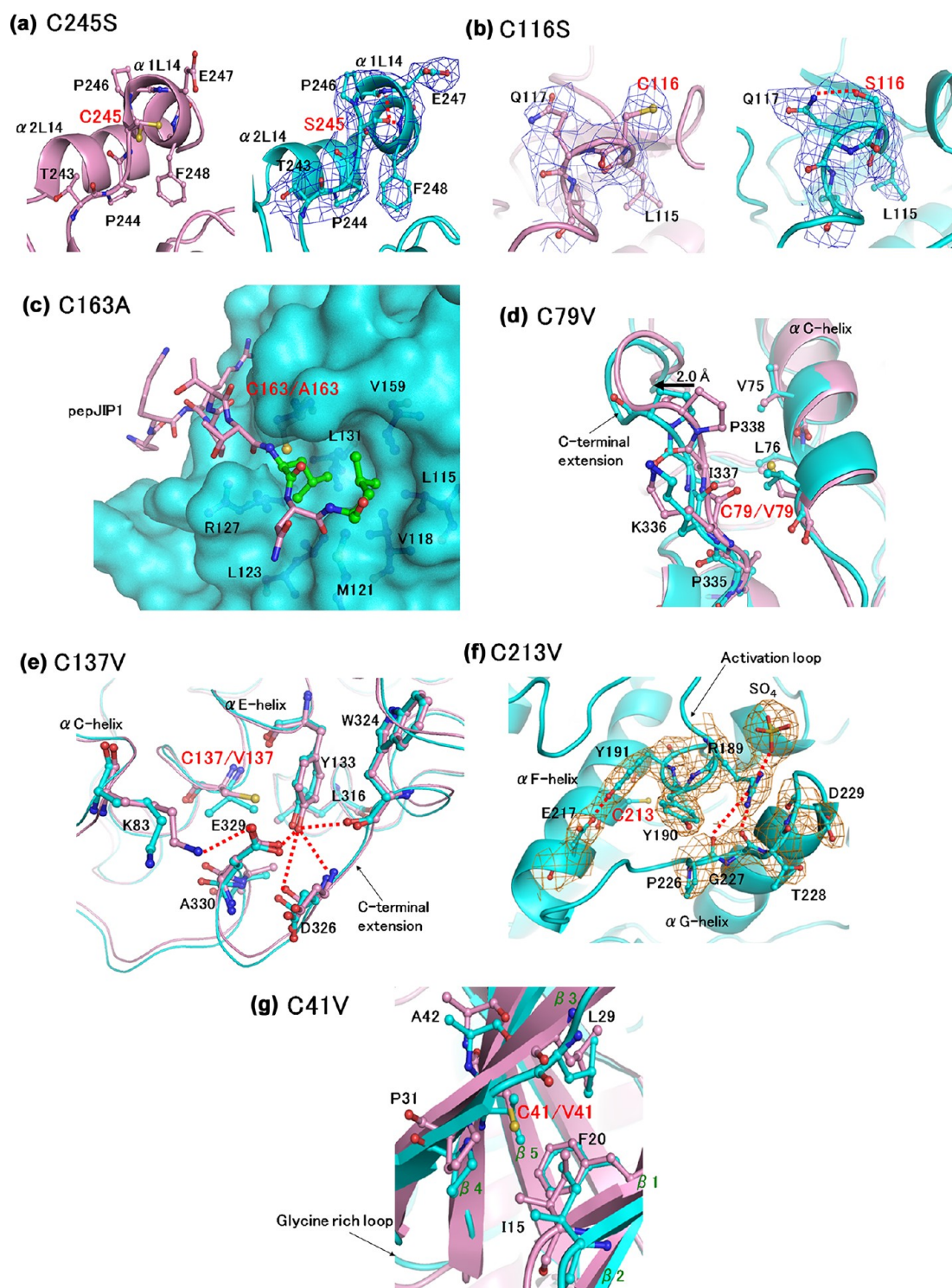


Figure 7. Structures of the seven cysteine-deficient mutation sites. (a) C245S site, superimposition of the wild-type structure (pink, PDB entry 3elj) and M1 (cyan). (b) C116S site, superimposition of M1 (pink) and M2 (cyan). (c) C163A site, M3 structure binding with pepJIP1. The molecular surface of M3 is colored cyan, and pepJIP1 is represented by the pink stick model. The hydrophobic residues in the substrate recognition pocket are represented as magenta sticks. (d) C79V site, superimposition of the wild-type structure (pink, PDB entry 3elj) and M4 (cyan). (e) C137V site, superimposition of M4 (pink) and M5 (cyan). (f) C213V site. (g) C41V site, superimposition of M6 (pink) and M7 (cyan). The hydrogen bonds are represented by green dashed lines. The $2F_o - F_c$ electron density map contoured at 1σ is colored blue in panels a and b and orange in panel f.

The second surface mutation (C116S in M2) additionally introduced into M1 further intensified the T_{m1} value but not T_{m2} . The kinase activity was retained but slightly decreased (-11%) in comparison with that of M1 (Table 3). T_{m1} was increased by this mutation in an enthalpy-dependent manner (Table 3), as well as

the C245S mutation. The thermal stabilization was acquired by the hydration on the mutated serine as well as the hydrogen bond formation of Ser116 (Figure 7b). However, the C116S/C245S double mutation was also insufficient for stabilizing the chemical properties of JNK1 and did not maximize the production yield.

The C163A surface mutation of JNK1 (in M3) significantly enhanced the chemical stability of the protein (Figure 3) and production yield (Table S2 of the Supporting Information). However, the C163A mutation conferred a modest destabilization of thermal stability (Table 3). The void volume created due to the C163A mutation might modestly destabilize the hydrophobic substrate-recognizing pocket and subsequently decrease the T_{m1} value without altering enzyme activity (Figure 7c).

The C79V mutation in M4 gave no improvement or deterioration to JNK1 and negligible adverse effects with respect to T_{m1} thermal stability. On the other hand, the DSC experiments implied that Cys79 likely plays a significant role in the T_{m2} transition, whereas the other cysteine residues are associated with the change in the T_{m1} transition (Table 3). The crystal structures support these thermodynamic phenomena. The $C\gamma$ atom of Val79 possibly creates repulsive forces with the backbone carbonyl O atom of Lys336 in the C-terminal extension (Figure 7d). This repulsive force is likely to destabilize the interaction of helix αC with the C-terminal extension and leads to the observed changes in the T_{m2} transition for the M4 mutant, yet no adverse effect on the enzyme activity was observed for M4.

The C137V mutation in M5 drastically reduced T_{m1} and enzyme activity but not T_{m2} . This result suggests that the T_{m1} transition is critical for retaining biological activity. The C137V mutation destabilized the hydrophobic cluster and the salt bridge that accompanies the hydrogen bond network of the C-lobe (Figure 7e) that represents a platform for substrate binding. Consequently, the C137V mutation drastically destabilized the structure and thus caused a decrease in enzyme activity.

The C213V mutation as well as the C137V mutation significantly reduced T_{m1} and enzyme activity but not T_{m2} . The movement of the hydrophobic core caused by the C213V mutation destabilized the hydrogen bond network (Figures 6c and 7f). Consequently, helices αF and αG , known as the MAP kinase insertion and involved in the other substrate binding site, were moved away toward the solvent. Therefore, the observed structural destabilization appears to have dramatically increased the amount of unfolded protein and therefore the amount of protein that was expressed in the insoluble fraction.

The C41V mutation as well as the C79V mutation gave no improvement or deterioration of the properties of JNK1 and moderately decreased the T_{m1} value. The M7 structure indicated that the C41V mutation was tolerated by the high flexibility in the glycine-rich loop region. This structural observation is consistent with the biological result that the mutation had a negligible effect on enzyme activity.

All cysteine-deficient mutations enforced structural changes and had desirable or adverse effects on the thermal stability of JNK1. On the basis of ΔT_m values for the T_{m1} transition, the C245S and C116S mutations are stabilizing, the C79V mutation is neutral, and the C163A, C137V, C213V, and C41V mutations are destabilizing (T_{m1}). On the basis of ΔT_m values for the T_{m2} transition, the C245S, C116S, C163A, C137V, C213V, and C41V mutations are neutral, and the C79V mutation is the only residue destabilizing the T_{m2} transition. These experimental results suggest that the C-lobe and the glycine-rich loop in the N-lobe are attributed to the T_{m1} transition domain, and the other part of the N-lobe is assigned to the T_{m2} transition domain, and that each transition is likely to occur independently. The T_{m1} transition domain involves the substrate peptide and ATP binding sites (Figure 5 and Table S3 of the Supporting Information). The JIP1 peptide that binds specifically to the C-lobe domain elevated the thermal stability represented by the T_{m1}

value, whereas the T_{m2} transition domain involves the backside of the active site and was not affected by peptide binding. The dissection concerning the transition domains implies that the addition of any interaction stabilizing the T_{m1} transition domain is allowed to stabilize the JNK1 structure, and thus, improvement by other mutations of the T_{m1} transition domain deserves further investigation.

From the point of view of enzymatic activity, the C245S mutation is a gain of function mutation, the C163A, C79V, and C41V mutations are neutral for function, and the C116S, C137V, and C213V mutations are negative for function. It seems that buried C137 and C213 may be a key for function; C79 and C41 can be substituted without an apparent effect upon function. Because the reduction in the T_{m1} value in M5 and M6 mutants reduced the kinase activity and the reduction of T_{m2} seen with the C79V mutation (Table 3) showed no effect on enzyme activity (Table 3), it seems that T_{m1} values (in M1–M4) are important for retaining kinase activity. The contribution of T_{m1} to retaining enzyme activity is also underpinned by the result that the T_{m1} shifted to a higher value via addition of the peptide (Figure 5).

Advantages of Cysteine-Deficient Mutants of Recombinant JNK1. The cysteine-deficient mutations improved the chemical stability of the JNK1 protein. In particular, replacement of all surface cysteines enhanced the chemical stability to quite a large extent (Figure 3). Because buried cysteine mutations had no effect on the chemical stability under the conditions of the series of the experiments performed (Figure 3), it is suggested that the surface cysteine residues promoted oligomerization whereas the buried cysteine residues did not participate in the oligomerization (Figure 3).

The decrease in the level of oligomerization by surface cysteine mutations seems to give a great advantage with higher production yields. Indeed, the increasing number of cysteine mutations gradually improved the protein production yield until the third mutation (Table S2 of the Supporting Information). Thereafter, additional mutations conferred no improvement or had an adverse effect on the yield (Table S2 of the Supporting Information). In other words, all surface mutations, C245S, C116S, and C163A (M1–M3), enhanced production yields. The expression of M3 occurred predominantly in the soluble fraction (Figure 2b) and thereby conferred the largest amount of purified material. Subsequently, the first buried cysteine mutation, C79V (M4), retained a production yield that was similar to the yields obtained for M3. The second buried cysteine mutation, C137V (M5), gave rise to a moderately adverse effect on the production yield, whereas the third and fourth buried cysteine mutations, C213V and C41V (M6 and M7), respectively, drastically reduced production yields. The production yields of these cysteine mutants were noticeably associated with the recovery in the soluble fraction of the JNK1 protein. The increase in the insoluble fraction led to a decrease in the production yield of the wild-type or mutant protein (Figure 2c and Table S2 of the Supporting Information). In the production of bacteria, the insoluble protein consists of unfolded or aggregated components triggered by the intra- and intermolecular disulfide bond formation and non-specific hydrophobic associations.²³ The improved production yields particularly seen in the M3 and M4 mutants are considered to originate from the combinational advantage of the chemical and/or thermal stabilities of these mutants, in which chemical stabilization protects the oxidation of surface cysteine residues and thermal stabilization improves the recovery of the soluble form of JNK1.

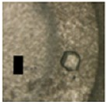

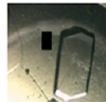


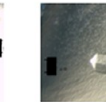
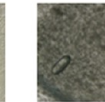
	M1	M2	M3	M4	M5	M6	M7
Crystals							
Crystals size (μm)	70×50×50	70×50×50	900×500×100	850×500×70	600×350×80	200×80×50	120×50×40
amorphous	++	+	–	–	+	+	++
Chemical stability	–	–	+	+	+	+	++
Thermal Stability	+	++	+	–	–	–	–

Figure 8. Impact of the seven cysteine-deficient mutations on the chemical and thermal stabilities in the crystallization experiment. To evaluate the amount of precipitant, the plus sign indicates the degree of precipitation and minus sign represents a small amount of precipitation. Chemical stability estimated by the nonreduced SDS–PAGE experiments is shown by the plus sign. Thermal stability determined by the T_{m1} and T_{m2} is shown by the plus sign as a stabilized state and by the minus sign as a destabilized state.

The stable JNK1 mutant gives us reason to investigate its interaction with drug candidates by structural biology approaches. The crystal size and the amount of precipitant of the seven cysteine-deficient mutants indicated that both chemical and thermal stabilities were essential for maintaining the stability of the protein over a long period. Smaller crystals were acquired in M1, M2, M6, and M7 with a large amount of protein precipitant observed compared with that of M3 (Figure 8). The non-reduced SDS–PAGE experiments implied that by chemical instability, the M1 and M2 mutants even with higher thermal stability were found to unfold and precipitate in the crystallizing solution, and the crystal growth of these mutants was therefore terminated. On the other hand, the DSC experiments conferred that by thermal instability, the M6 and M7 mutants even with higher chemical stability behaved the same as the M1 and M2 mutants. Consequently, the M3 mutant with both chemical and thermal stabilities was the most stable during the crystallization process, and thus, the largest crystals were obtained for this mutant. Replacements of surface cysteine residues of JNK1 also allow us to evaluate reliably the interaction between JNK1 and drug candidates, especially in using physicochemical techniques.

Design of Cysteine-Deficient Mutations To Reserve Enzymatic Activity and Protein Stability. The contribution of each cysteine-deficient mutation to thermal stability varies based upon the accessible surface area [ASA (Table 1)] of the $S\gamma$ atom of cysteine, which is classified into three categories, buried ($ASA = 0 \text{ \AA}^2$), partially accessible ($ASA < 10 \text{ \AA}^2$), and accessible ($ASA \gg 10 \text{ \AA}^2$) cysteine residues. Buried cysteine residue Cys83 of fibroblast growth factor-1 (FGF1) cannot be replaced with alanine, serine, threonine, or valine without major effects on thermal stability, although the C83S and C83T mutations of FGF1 moderately enhanced the physiological half-life.^{23,24,38} Likewise, the C137V and C213V mutations of JNK1 collapsed the hydrophobic core and conferred major destabilization with the reduction of the enzyme function, indicating that the cysteine residues in the highly rigid region of JNK1 and FGF1 are hard to replace with the other amino acid without a loss of thermal stability. On the other hand, the valine substitutions of buried cysteine residues Cys41 and Cys79 in the flexible region of JNK1 retained enzymatic function, but the effects on thermal stability were different (i.e., slight destabilization in C41V and destabilization in C79V). Altogether, the thermal stability of the buried cysteine-deficient mutant seems to be extensively altered

depending on the structural flexibility around the relevant cysteine residue.

The partially accessible cysteine-deficient mutation has no effect or a moderate effect on thermal stability. The C163A mutation of JNK1 resulted in a moderate destabilization of the structure (Table 3). However, the JIP1 peptide increased the T_{m1} transition temperature of M3 and the wild type (Figure 5), and thus, this mutation had little adverse effect on substrate recognition. The C163A mutation retained enzyme activity compared with the M2 mutant and wild-type protein (Table 3), whereas the C162S mutation of the p38 α MAP kinase had significantly reduced enzyme activity.²⁵ The crystal structure revealed that the mutated serine residue of p38 α altered the configuration of the hydrophobic pocket where the substrate was recognized.²⁵ The modeling study revealed that the C163V mutation of JNK1 would narrow the hydrophobic substrate-recognizing pocket and likely reduce the activity as well as the p38 α C162S mutation. The C117S and C117I mutations of FGF1 moderately decreased thermal stability, but the C117V mutation retained that.^{24,38,39} The hydrophobic pocket proximate to the $S\gamma$ atom of Cys117 ($ASA = 9.7 \text{ \AA}^2$) involving Val31, Leu72, and Leu73 of FGF1 likely accommodates the valine rather than the serine or isoleucine. Our results and the previous reports^{24,25,38,39} reveal that the mutation of the partially accessible cysteine possibly promotes chemical stability with no critical impact on thermal stability.

The accessible cysteine residues Cys116 and Cys245 of JNK1, which $S\gamma$ atoms were largely exposing to the solvent, were replaced with serine with enhancement of thermal stability (Table 3). Furthermore, our results suggested that this mutation certainly enhanced chemical stability (Figure 3). Therefore, the accessible cysteine should be a first target for stabilizing the protein sample.

The effect of the cysteine-deficient mutation on protein stability greatly varies with the combination of the structural flexibility and accessibility of the environment in which the $S\gamma$ atom of the cysteine residue is located. The results herein together with the previous results^{23–25,35,37–39} cover most aspects of the cysteine marginal environment and should provide a valuable approach for stabilizing proteins possessing free cysteine residues.

SUMMARY

We studied the role of the cysteine residues in the biological, chemical, and thermodynamic characteristics of JNK1, and the

results were interpreted with structural information. The roles of the cysteine residues in JNK1 were divided into three categories. The first category includes surface cysteine residues C245, C116, and C163. These residues have a negligible effect on the folding of the protein, except for local structural stabilization or destabilization. The C245S, C116S, and C163A mutations, each eliminating a surface reactive thiol (i.e., free cysteine residue), enhanced the chemical stability. The second category included the buried cysteine residues C41 and C79. Both residues are positioned in flexible regions and moderately contributed to the thermal stability; however, both residues had no effect on enzyme activity. Therefore, these two mutations enhanced the chemical stability and will give great advantages in physicochemical experiments used for the analysis of structure–function relationships and drug screenings. Finally, the third category includes the fully buried cysteine residues C137 and C213 in the tightly filled hydrophobic region. These residues contribute significantly to protein folding. Therefore, mutation of these residues decreased the enzyme activity of JNK1, yet these mutations promoted chemical stability.

The results presented here can be applied to other MAP kinases and, together with the previous results,^{23,35,37} to intracellular proteins possessing free cysteine residues. Finally, this technique should provide a valuable approach for increasing production yields and stabilizing MAP kinase samples. Such benefits should accelerate rational drug discovery.

■ ASSOCIATED CONTENT

■ Supporting Information

X-ray data collection and structure refinement statistics (Table S1), production yield of the wild type (M0) and cysteine-deficient mutants (M1–M7) (Table S2), and summary of thermodynamic transition parameters of M0, M3, and M7 from curve fitting of each DSC peak as a two-state transition (Table S3). This material is available free of charge via the Internet at <http://pubs.acs.org>.

■ AUTHOR INFORMATION

Corresponding Author

*Fax: +81 72 254 9819. Telephone: +81 72 254 9819. E-mail: kinotk@b.s.osakafu-u.ac.jp.

Funding

This study was supported by a KAKENHI Grant-in-Aid for Scientific Research (C) (19S70111).

Notes

The authors declare no competing financial interest.

■ ACKNOWLEDGMENTS

The synchrotron radiation experiments were performed at the Photon Factory with the approval of the Japan Synchrotron Radiation Research Institute. We thank the staff for their help in the collection of data at the NE3A station.

■ ABBREVIATIONS

JNK, c-Jun N-terminal kinase; MAPK, mitogen-activated protein kinase; SBDD, structure-based drug design; DSC, differential scanning calorimetry; M0, wild-type JNK1; M1–M7, seven cysteine-deficient JNK1 mutants; JIP1, JNK interacting protein 1; DTT, dithiothreitol; MAP2K4, mitogen-activated protein kinase kinase 4; MAP2K7, mitogen-activated protein kinase kinase 7; PDB, Protein Data Bank.

■ REFERENCES

- (1) Cheng, Z., Zhang, J., Ballou, D. P., and Williams, C. H., Jr. (2011) Reactivity of thioredoxin as a protein thiol-disulfide oxidoreductase. *Chem. Rev.* 111, 5768–5783.
- (2) Mailloux, R. J., Seifert, E. L., Bouillaud, F., Aguer, C., Collins, S., and Harper, M. E. (2011) Glutathionylation acts as a control switch for uncoupling proteins UCP2 and UCP3. *J. Biol. Chem.* 286, 21865–21875.
- (3) Baker, L. M., and Poole, L. B. (2003) Catalytic mechanism of thiol peroxidase from *Escherichia coli*. Sulfenic acid formation and over-oxidation of essential CYS61. *J. Biol. Chem.* 278, 9203–9211.
- (4) Astier, J., Rasul, S., Koen, E., Manzoor, H., Besson-Bard, A., Lamotte, O., Jeandroz, S., Durner, J., Lindermayr, C., and Wendehenne, D. (2011) S-nitrosylation: An emerging post-translational protein modification in plants. *Plant Sci.* 181, 527–533.
- (5) Davis, R. J. (2000) Signal transduction by the JNK group of MAP kinases. *Cell* 103, 239–252.
- (6) Manning, A. M., and Davis, R. J. (2003) Targeting JNK for therapeutic benefit: From junk to gold? *Nat. Rev. Drug Discovery* 2, 554–565.
- (7) Hirosumi, J., Tuncman, G., Chang, L., Gorgun, C. Z., Uysal, K. T., Maeda, K., Karin, M., and Hotamisligil, G. S. (2002) A central role for JNK in obesity and insulin resistance. *Nature* 420, 333–336.
- (8) Jaeschke, A., Rincon, M., Doran, B., Reilly, J., Neuber, D., Greiner, D. L., Shultz, L. D., Rossini, A. A., Flavell, R. A., and Davis, R. J. (2005) Disruption of the Jnk2 (Mapk9) gene reduces destructive insulinitis and diabetes in a mouse model of type I diabetes. *Proc. Natl. Acad. Sci. U.S.A.* 102, 6931–6935.
- (9) Liang, Q., and Molkentin, J. D. (2003) Redefining the roles of p38 and JNK signaling in cardiac hypertrophy: Dichotomy between cultured myocytes and animal models. *J. Mol. Cell. Cardiol.* 35, 1385–1394.
- (10) Han, Z., Boyle, D. L., Aupperle, K. R., Bennett, B., Manning, A. M., and Firestein, G. S. (1999) Jun N-terminal kinase in rheumatoid arthritis. *J. Pharmacol. Exp. Ther.* 291, 124–130.
- (11) Han, Z., Boyle, D. L., Chang, L., Bennett, B., Karin, M., Yang, L., et al. (2001) c-Jun N-terminal kinase is required for metalloproteinase expression and joint destruction in inflammatory arthritis. *J. Clin. Invest.* 108, 73–81.
- (12) Kennedy, N. J., and Davis, R. J. (2003) Role of JNK in tumor development. *Cell Cycle* 2, 199–201.
- (13) Scapin, G., Patel, S. B., Lisnock, J., Becker, J. W., and LoGrasso, P. V. (2003) The structure of JNK3 in complex with small molecule inhibitors: Structural basis for potency and selectivity. *Chem. Biol.* 10, 705–712.
- (14) Liu, M., Xin, Z., Clapit, J. E., Wang, S., Gum, R. J., Haasch, D. L., Trevillyan, J. M., Abad-Zapatero, C., Fry, E. H., Sham, H. L., and Liu, G. (2006) Synthesis and SAR of 1,9-dihydro-9-hydroxypyrazolo[3,4-b]quinolin-4-ones as novel, selective c-Jun N-terminal kinase inhibitors. *Bioorg. Med. Chem. Lett.* 16, 2590–2594.
- (15) Zhao, H., Serby, M. D., Xin, Z., Szczepankiewicz, B. G., Liu, M., Kosogof, C., Liu, B., Nelson, L. T., Johnson, E. F., Wang, S., Pederson, T., Gum, R. J., Clapit, J. E., Haasch, D. L., Abad-Zapatero, C., Fry, E. H., Rondinone, C., Trevillyan, J. M., Sham, H. L., and Liu, G. (2006) Discovery of potent, highly selective, and orally bioavailable pyridine carboxamide c-Jun NH₂-terminal kinase inhibitors. *J. Med. Chem.* 49, 4455–4458.
- (16) Liu, M., Wang, S., Clapit, J. E., Gum, R. J., Haasch, D. L., Rondinone, C. M., Trevillyan, J. M., Abad-Zapatero, C., Fry, E. H., Sham, H. L., and Liu, G. (2007) Discovery of a new class of 4-anilinopyrimidines as potent c-Jun N-terminal kinase inhibitors: Synthesis and SAR studies. *Bioorg. Med. Chem. Lett.* 17, 668–672.
- (17) Chamberlain, S. D., Redman, A. M., Wilson, J. W., Deanda, F., Shotwell, J. B., Gerding, R., Lei, H., Yang, B., Stevens, K. L., Hassell, A. M., Shewchuk, L. M., Leesnitzer, M. A., Smith, J. L., Sabbatini, P., Atkins, C., Groy, A., Rowand, J. L., Kumar, R., Mook, R. A., Jr., Moorthy, G., and Patnaik, S. (2009) Optimization of 4,6-bis-anilino-1H-pyrrolo[2,3-d]pyrimidine IGF-1R tyrosine kinase inhibitors towards JNK selectivity. *Bioorg. Med. Chem. Lett.* 19, 360–364.

- (18) Mateja, A., Devedjiev, Y., Krowarsch, D., Longenecker, K., Dauter, Z., Otlewski, J., and Derewenda, Z. S. (2002) The impact of Glu→Ala and Glu→Asp mutations on the crystallization properties of RhoGDI: The structure of RhoGDI at 1.3 Å resolution. *Acta Crystallogr. D58*, 1983–1991.
- (19) Charron, C., Kern, D., and Giege, R. (2002) Crystal contacts engineering of aspartyl-tRNA synthetase from *Thermus thermophilus*: Effects on crystallizability. *Acta Crystallogr. D58*, 1729–1733.
- (20) Nickerson, D., Wong, L. L., and Rao, Z. (1998) An improved procedure for the preparation of X-ray diffraction-quality crystals of cytochrome p450cam. *Acta Crystallogr. D54*, 470–472.
- (21) Schwede, T. F., Badeker, M., Langer, M., Retey, J., and Schulz, G. E. (1999) Homogenization and crystallization of histidine ammonia-lyase by exchange of a surface cysteine residue. *Protein Eng. 12*, 151–153.
- (22) Hibi, T., Hisada, H., Nakatsu, T., Kato, H., and Jun'ichi, O. H. (2002) *Escherichia coli* B γ -glutamylcysteine synthetase: Modification, purification, crystallization and preliminary crystallographic analysis. *Acta Crystallogr. D58*, 316–318.
- (23) Lee, J., and Blaber, M. (2009) The interaction between thermodynamic stability and buried free cysteines in regulating the functional half-life of fibroblast growth factor-1. *J. Mol. Biol. 393*, 113–127.
- (24) Culajay, J. F., Blaber, S. I., Khurana, A., and Blaber, M. (2000) Thermodynamic characterization of mutants of human fibroblast growth factor 1 with an increased physiological half-time. *Biochemistry 39*, 7153–7158.
- (25) Patel, S. B., Cameron, P. M., Frantz-Wattley, B., O'Neill, E., Becker, J. W., and Scapin, G. (2004) Lattice stabilization and enhanced diffraction in human p38 α crystals by protein engineering. *Biochim. Biophys. Acta 1696*, 67–73.
- (26) Shaw, D., Wang, S. M., Villaseñor, A. G., Tsing, S., Walter, D., Browner, M. F., Barnett, J., and Kuglstatter, A. (2008) The crystal structure of JNK2 reveals conformational flexibility in the MAP kinase insert and indicates its involvement in the regulation of catalytic activity. *J. Mol. Biol. 383*, 885–893.
- (27) Bradford, M. M. (1976) A rapid and sensitive method for the quantitation of microgram quantities of protein utilizing the principle of protein-dye binding. *Anal. Biochem. 72*, 248–254.
- (28) Sturtevant, J. M. (1987) Biochemical applications of differential scanning calorimetry. *Annu. Rev. Phys. Chem. 38*, 463–488.
- (29) Otwinowski, Z. (1993) Oscillation data reduction program. In *Proceedings of the CCP4 Study Weekend: Data collection and processing* (Sawyer, L., et al., Eds.) pp 56–62, Daresbury Laboratory, Warrington, U.K.
- (30) Vagin, A., and Teplyakov, A. (1997) MOLREP: An automated program for molecular replacement. *J. Appl. Crystallogr. 30*, 1022–1025.
- (31) Collaborative Computational Project, Number 4 (1994) CCP4 suite: Programs for protein crystallography. *Acta Crystallogr. D50*, 760–763.
- (32) Emsley, P., and Cowtan, K. (2004) Coot: Model-building tools for molecular graphics. *Acta Crystallogr. D60*, 2126–2132.
- (33) Laskowski, R. A., MacArthur, M. W., Moss, D. S., and Thornton, J. M. (1993) PROCHECK: A program to check the stereochemical quality of protein structures. *J. Appl. Crystallogr. 26*, 283–291.
- (34) Heo, Y. S., Kim, S. K., Seo, C. I., Kim, Y. K., Sung, B. J., Lee, H. S., Lee, J. I., Park, S. Y., Kim, J. H., Hwang, K. Y., Hyun, Y. L., Jeon, Y. H., Ro, S., Cho, J. M., Lee, T. G., and Yang, C. H. (2004) Structural basis for the selective inhibition of JNK1 by the scaffolding protein JIP1 and SP600125. *EMBO J. 23*, 2185–2195.
- (35) Yutani, K., Ogasahara, K., Tsujita, T., and Sugino, Y. (1987) Dependence of conformational stability on hydrophobicity of the amino acid residue in a series of variant proteins substituted at a unique position of tryptophan synthase α subunit. *Proc. Natl. Acad. Sci. U.S.A. 84*, 4441–4444.
- (36) Miller, S., Janin, J., Lesk, A. M., and Chothia, C. (1987) Interior and surface of monomeric proteins. *J. Mol. Biol. 196*, 641–656.
- (37) Matsumura, M., Becktel, W. J., and Matthews, B. W. (1988) Hydrophobic stabilization in T4 lysozyme determined directly by multiple substitutions of Ile 3. *Nature 334*, 406–410.
- (38) Lee, J., and Blaber, M. (2009) Structural basis of conserved cysteine in the fibroblast growth factor family: Evidence for a vestigial half-cysteine. *J. Mol. Biol. 393*, 128–139.
- (39) Brych, S. R., Kim, J., Logan, T. M., and Blaber, M. (2003) Accommodation of a highly symmetric protein superfold. *Protein Sci. 12*, 2704–2718.
- (40) Tsodikov, O. V., Record, M. T., and Sergeev, Y. V. (2002) Novel computer program for fast exact calculation of accessible and molecular surface areas and average surface curvature. *J. Comput. Chem. 23*, 600–609.